Interference of guided modes in a two-port ring waveguide composed of dielectric nanoparticles

I. Ya. Polishchuk
Max-Planck-Institut für Physik Komplexer Systeme, D-01187 Dresden, Germany; RRC Kurchatov Institute, Kurchatov Sq., 1, 123182 Moscow, Russia; and Department of Chemistry, Tulane University, New Orleans, Louisiana 70118, USA

M. I. Gozman
RRC Kurchatov Institute, Kurchatov Sq., 1, 123182 Moscow, Russia and Department of Chemistry, Tulane University, New Orleans, Louisiana 70118, USA

Gail S. Blaustein and A. L. Burin
Department of Chemistry, Tulane University, New Orleans, Louisiana 70118, USA
(Received 22 October 2008; revised manuscript received 27 October 2009; published 16 February 2010)

The interference is considered of guided polariton modes in a two-port ring waveguide composed of dielectric nanospheres. The dependence of the guided polariton intensity on the relative orientation of the input and output channels is investigated. It is shown that, if the frequency of the external light source corresponds to one of the resonant modes of the waveguide ring segment, the guided polariton may be treated as two optical beams running along the ring segment in the opposite directions and interfering with each other. The multisphere Mie scattering formalism is used. The dipole approximation is shown to grasp the essence of physics. Our simple interpretation of the results is obtained in terms of scalar waves. The applications of the interference revealed in the manuscript are discussed as well.

DOI: 10.1103/PhysRevE.81.026601 PACS number(s): 41.20.Jb, 42.25.Hz, 42.60.Da, 42.79.Gn

I. INTRODUCTION

Low-dimensional aggregates of nanoparticles absorbing, scattering and transmitting electromagnetic waves attract the growing interest because they can be used in various microsystems and nanosystems, in which optical energy can be received, converted, and transferred on a subwavelength scale [1–17]. The linear or circular arrays of spherical dielectric particles are an important branch of these investigations [1–5,14,16,17]. If the material refractive index is sufficiently large ($n_r > 2$), these arrays can possess long-living quasistates [14,16]. They are *polariton* modes representing a superposition of light and material polarization oscillation. Within the frequency interval in which the material absorption is small, the losses due to emission of a free photon are still possible. However, for sufficiently large sizes of the aggregates these losses vanish [5,14,16]. Thus, the systems under consideration can be used as waveguides for optical energy transport. The transferred energy, in particular, can stimulate a number of processes such as photoexcitation of molecules or chemical reactions [12,13].

To our knowledge, first nanowaveguides capable of transferring optical energy at the distance of a hundred nanometers were constructed by Atwater and coworkers as a linear chain of spherical silver or gold particles [9,10,12,13]. Metallic particles can easily be made much smaller than the traveling light wavelength in vacuum (low diffraction threshold in the optical region) [12]. The waveguides composed of these particles possess the propagating modes with the vanishing radiation loss. This takes place for the modes with the dispersion law obeying the condition $\omega(k) < ck$ to be called a *guided mode criterion* [see Eq. (10) below]. Here, $\omega(k)$ is a frequency of a propagating mode, k is a wave vector of the mode, c is velocity of light in free space. According to [14–17], the longer the array, the smaller the radiation losses. This conclusion is valid for both metal and dielectric waveguides. However, the guided mode criterion is important only for dielectric arrays since the absorption losses inherent in metals exceed the radiation ones by one or two orders of magnitude.

In the present paper, we consider dielectric waveguides, which are free of the absorption losses. Thus, the main mechanism responsible for polariton decay is the polariton-free photon conversion [14–17].

The long-living polariton states form a pass band [17], being the analog of the conductivity band in conventional crystals. The pass band is a frequency domain in which a polariton propagates over the waveguide without radiation losses. For the sufficiently long chain, the pass band practically coincides with the pass band of the infinite chain. In the latter case, the top of the frequency pass band corresponds to the Brillouin zone boundary in the quasimomentum space [15–17]. The bottom of the frequency pass band is determined by the condition $\omega(k)=ck$, which follows from the guided mode criterion [17]. The different pass bands are separated by the forbidden bands analogous to those in conventional crystals.

The long-living polaritons can be generated by a monochromatic point light source located near a waveguide. It has been established that, the closer the source frequency to the top of the pass band, the smaller the polariton decay rate γ. In particular, for the linear arrays of N spherical particles $\gamma(N) \sim N^{-3}$ [16]. For circular arrays of spherical particles $\ln \gamma^{-1}(N) \sim N$ [14]. The last dependence has also been established for the circular arrays of cylindrical antennas [18–20]. This allows us to expect that the results obtained in the paper for the arrays of spherical particles can be applied to arrays composed of cylindrical particles as well.

It is well known that under certain circumstances a Bloch electron excitation can propagate coherently over a fine wire. One remarkable manifestation of this fact is the interference of two such electron excitations. E.g., the interference of two

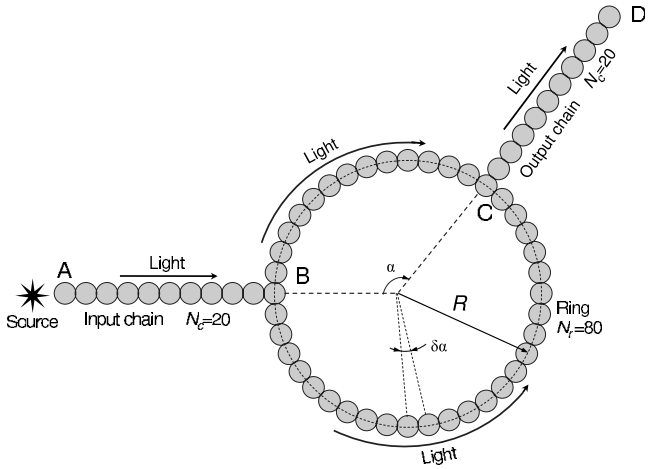

FIG. 1. A two-port ring waveguide composed of spherical particles. N_r is the number of particles in the ring. N_c is the number of particles in the input and output chains.

electron excitations traveling in the opposite directions in fine metallic rings is used in measuring devices such as SQUIDS. Due to close similarity between polariton and electron excitations, one can expect that a number of features inherent in the coherent propagation of electric current in fine metallic wires will show up in optical waveguides. The main goal of the manuscript is to elucidate how the interference, if any, affects the propagation of the optical excitation through a two-port ring waveguide composed of dielectric nanoparticles (see Fig. 1 below).

Note that the problem similar to that in the present paper was considered for microstrip optical and microwave ring resonators in [21–23]. However, the resonators investigated in those papers were just the conventional fibers with the constant diameter larger than the light wavelength inside the resonators. In contrast, the main feature of the systems investigated here is that they are composed of small identical spheres. Also, the diameter of these spheres, i.e., lateral dimension of the waveguide under consideration, is of the order of a wavelength. In addition, the array we consider is a periodic one and possesses a band structure where the polariton group velocity vanishes at the Brillouin band edge, forming a slow light mode [16]. Thus, our two-port ring waveguide essentially differs from the resonators considered in [21–23]. Despite these differences, the resonances inherent in the ring part of the array are of the same nature as in [21–23].

In our study we consider GaAs particles having refractive index n_r=3.5. This material possesses one of highest refractive indices amongst conventional optical materials and consequently possesses excellent guiding properties (cf [14,16,17]). However, absorption by GaAs is negligible only in the infrared spectral domain [24].

In this manuscript, we are interested in the pass band possessing the lowest frequencies. In addition, we are interested in the polariton modes close to the top edge of this band. The later stems from the fact that, the closer the mode to the upper edge, the higher the mode quality factor. In our case these modes are *transverse magnetic dipole* modes [14,16,17]. For this reason, we use a point magnetic dipole light source directed normally to the plane of the waveguide.

In Sec. II, we describe a two-port ring waveguide and a ring waveguide considered in the paper. Their guided properties are investigated using the multisphere Mie scattering formalism (MSMSF) [25–27]. This formalism is introduced in Sec. III where we also describe the calculations of the polariton dispersion law. In Sec. IV, the formalism is applied to investigating the interference in the waveguides. The dipole approximation justified in our previous works [14–17] is used and we truncate the systems of equations described in Sec. III, accordingly. In Sec. V, we propose a simple physical picture based on the interference of scalar Bloch waves to treat the results of the numerical simulation. In Sec. VI, the results are summarized and their applications to various systems of interest are discussed.

II. TWO-PORT RING WAVEGUIDE AND RING WAVEGUIDE

A two-port ring waveguide to be considered in the paper is represented in Fig. 1. The two-port ring waveguide, instead of an ordinary ring waveguide, is chosen for the analysis because this configuration is closer to the real waveguide geometry. The linear chains *AB* and *CD* provide the input and output channels while the ring connecting them employs the interference to control the transport of waves through the waveguide. The expected interference is due to two polaritons traveling in the ring segment from point *B* to point *C* clockwise and counterclockwise respectively.

To investigate the light propagation over the waveguide, let us place a point light source in the beginning of the input chain (near the point *A* in Fig. 1). A polariton, created by this source, travels along the chain *AB* to the point *B*. In this point the polariton splits into two polaritons moving along the ring to the point *C* in the opposite directions, clockwise, and counterclockwise. These polaritons rejoin in the point *C*. Then, the rejoined polariton travels to the point *D* along the chain *CD*. Since the optical path lengths for the polaritons traveling in the opposite directions between the points *B* and *C* differ, the interference in the point *C* results in the polariton amplitude dependent on the angle α between the chains (see. Fig. 1). Therefore, the polariton amplitude at the point *D* also depends on the angle α. Finding this dependence is the main goal of the paper. We expect that this dependence is mainly determined by the ring part of the waveguide. However, one should reveal how the input and the output chains influence the interference. To do this, we remove the chains and place the point light source near the point *B* (see Fig. 2).

Then, we investigate how the polariton amplitude at the point *C* depends on the angle α. We show that the behavior of the polariton amplitudes in the points *D* and *C*, for the two-port ring and the ordinary ring, respectively, is qualitatively similar. The similarity shows up at the frequencies corresponding to discrete resonances for the ring [14] where the polariton amplitude depends remarkably on the angle α (position on the ring). This dependence is approximately periodic, with an angular period of the order of tens $\delta\alpha = 2\pi/N_r$, N_r being the number of spheres in the ring segment. The proper explanation is given below based on the simple

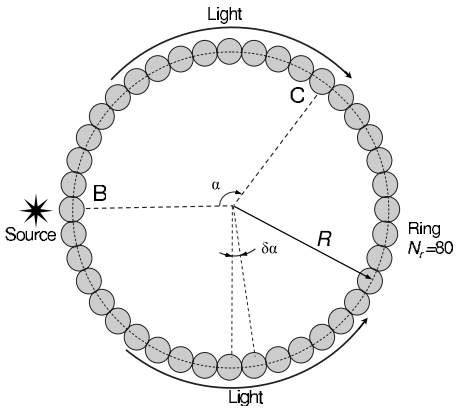

FIG. 2. A ring waveguide composed of N_r spherical particles.

physical argument which proves the existence of the interference.

III. MULTISPHERE MIE SCATTERING FORMALISM

A. General formalism

Let $\mathbf{E}_{inc}(\mathbf{r},\omega)$ and $\mathbf{H}_{inc}(\mathbf{r},\omega)$ be the monochromatic wave incident on the array of spheres. For the sake of simplicity, below the argument ω is omitted. Let $\mathbf{r}_j$ be the center of the j-th particle, $j=1,\ldots,N$, where N is the total number of particles in the array. The incident wave may be represented as a linear combination of vector spherical harmonics $\mathbf{N}_{mn}^{(1)}(\mathbf{r})$ and $\mathbf{M}_{mn}^{(1)}(\mathbf{r})$ being taken with respect to the center of an arbitrary j-th sphere [25,26] so that

$$\mathbf{E}_{inc}(\mathbf{r}) = \sum_{n=1}^{+\infty}\sum_{m=-n}^{n} i[p_{mn}^{j}\mathbf{N}_{mn}^{(1)}(\mathbf{r}-\mathbf{r}_j) + q_{mn}^{j}\mathbf{M}_{mn}^{(1)}(\mathbf{r}-\mathbf{r}_j)],$$

$$\mathbf{H}_{inc}(\mathbf{r}) = \sum_{n=1}^{+\infty}\sum_{m=-n}^{n} [q_{mn}^{j}\mathbf{N}_{mn}^{(1)}(\mathbf{r}-\mathbf{r}_j) + p_{mn}^{j}\mathbf{M}_{mn}^{(1)}(\mathbf{r}-\mathbf{r}_j)]. \quad (1)$$

Here, $n=1,\ldots,+\infty$ stands for the angular momenta of vector spherical harmonics, and $m=-n,\ldots,n$ is the projection of angular momentum on the z axis. The vector spherical harmonics depend on the parameter ω. The partial amplitudes of the incident wave p_{mn}^{j}, q_{mn}^{j} are the setup parameters for our task.

Let $\mathbf{E}_{sca}^{j}(\mathbf{r})$ and $\mathbf{H}_{sca}^{j}(\mathbf{r})$ be wave scattered by the j-th sphere. Following [25–27], it is convenient to expand this wave over vector spherical harmonics $\mathbf{N}_{mn}^{(3)}(\mathbf{r})$ and $\mathbf{M}_{mn}^{(3)}(\mathbf{r})$. So we have

$$\mathbf{E}_{sca}^{j}(\mathbf{r}) = \sum_{n=1}^{+\infty}\sum_{m=-n}^{n} i[a_{mn}^{j}\mathbf{N}_{mn}^{(3)}(\mathbf{r}-\mathbf{r}_j) + b_{mn}^{j}\mathbf{M}_{mn}^{(3)}(\mathbf{r}-\mathbf{r}_j)],$$

$$\mathbf{H}_{sca}^{j}(\mathbf{r}) = \sum_{n=1}^{+\infty}\sum_{m=-n}^{n} [b_{mn}^{j}\mathbf{N}_{mn}^{(3)}(\mathbf{r}-\mathbf{r}_j) + a_{mn}^{j}\mathbf{M}_{mn}^{(3)}(\mathbf{r}-\mathbf{r}_j)]. \quad (2)$$

Here a_{mn}^{j}, b_{mn}^{j} are partial amplitudes for the outgoing waves scattered by the j-th particle. These amplitudes obey a set of equations [25–27]

$$\frac{a_{mn}^{j}}{\bar{a}_n^j} + \sum_{l=1(l\neq j)}^{N}\sum_{\nu=1}^{+\infty}\sum_{\mu=-\nu}^{\nu}(A_{mn\mu\nu}^{lj}a_{\mu\nu}^{l} + B_{mn\mu\nu}^{lj}b_{\mu\nu}^{l}) = -p_{mn}^{j},$$

$$\frac{b_{mn}^{j}}{\bar{b}_n^j} + \sum_{l=1(l\neq j)}^{N}\sum_{\nu=1}^{+\infty}\sum_{\mu=-\nu}^{\nu}(A_{mn\mu\nu}^{lj}b_{\mu\nu}^{l} + B_{mn\mu\nu}^{lj}a_{\mu\nu}^{l}) = -q_{mn}^{j}. \quad (3)$$

Here $\bar{a}_n^j$ and $\bar{b}_n^j$ are the Mie coefficients, which determine the scattered field. They depend on the frequency, size and refractive index for the j-th particle [25,26]. The vector translation coefficients $A_{mn\mu\nu}^{lj}$ and $B_{mn\mu\nu}^{lj}$ depend on the frequency and the relative position of the j-th and l-th particles. They describe the retarded multipole interaction between these particles in the frequency domain.

Suppose that the incident field, see Eq. (1), is due to point light source placed at point $\mathbf{r}_0$. Then, the incident wave may be expressed as a linear combination of the vector spherical harmonics,

$$\mathbf{E}_{inc}(\mathbf{r}) = \sum_{n=1}^{+\infty}\sum_{m=-n}^{n} i[P_{mn}\mathbf{N}_{mn}^{(3)}(\mathbf{r}-\mathbf{r}_0) + Q_{mn}\mathbf{M}_{mn}^{(3)}(\mathbf{r}-\mathbf{r}_0)],$$

$$\mathbf{H}_{inc}(\mathbf{r}) = \sum_{n=1}^{+\infty}\sum_{m=-n}^{n} [Q_{mn}\mathbf{N}_{mn}^{(3)}(\mathbf{r}-\mathbf{r}_0) + P_{mn}\mathbf{M}_{mn}^{(3)}(\mathbf{r}-\mathbf{r}_0)]. \quad (4)$$

The coefficients p_{mn}^{j} and q_{mn}^{j} are connected with the coefficients P_{mn} and Q_{mn} by means of the relations,

$$p_{mn}^{j} = \sum_{\nu=1}^{+\infty}\sum_{\mu=-\nu}^{\nu}(A_{mn\mu\nu}^{j0}P_{\mu\nu} + B_{mn\mu\nu}^{j0}Q_{\mu\nu}),$$

$$q_{mn}^{j} = \sum_{\nu=1}^{+\infty}\sum_{\mu=-\nu}^{\nu}(B_{mn\mu\nu}^{j0}P_{\mu\nu} + A_{mn\mu\nu}^{j0}Q_{\mu\nu}). \quad (5)$$

The translation coefficients $A_{mn\mu\nu}^{j0}$ and $B_{mn\mu\nu}^{j0}$ depend on the relative position of the source and the center of the corresponding sphere. Let us recall that we are interested in the transverse magnetic dipole modes. One has for the point magnetic dipole source $Q_{01}=1$, $Q_{-11}=Q_{11}=0$, $P_{-11}=P_{01}=P_{11}=0$, and $P_{mn}=Q_{mn}=0$ for $n>1$ [28]. Thus, Eq. (5) define the right-hand side (RHS) of Eq. (3).

The electrical field component *inside* the j-th sphere with the diameter D_j is given by the expression ([25,26])

$$\mathbf{E}^{j}(\mathbf{r}) = -\sum_{n=1}^{+\infty}\sum_{m=-n}^{n} i[d_{mn}^{j}\mathbf{N}_{mn}^{(1)}(\mathbf{r}-\mathbf{r}_j) + c_{mn}^{j}\mathbf{M}_{mn}^{(1)}(\mathbf{r}-\mathbf{r}_j)],$$

$$|\mathbf{r}-\mathbf{r}_j| < D_j/2, \quad (6)$$

$$c^j_{mn} = (\bar{c}^j_n/\bar{b}^j_n)b^j_{mn}, \quad d^j_{mn} = (\bar{d}^j_n/\bar{a}^j_n)a^j_{mn}. \tag{7}$$

Here $\bar{c}^j_n$ and $\bar{d}^j_n$ are the Mie coefficients which determine the field inside the j-th particle [25,26]. Then, the polariton amplitude is proportional to the polarization

$$\mathbf{P}^j(\mathbf{r}) = \frac{n_r^2 - 1}{4\pi}\mathbf{E}^j(\mathbf{r}). \tag{8}$$

Suppose all of the spheres from the array are identical and $D_j = a$, where a is a distance between the nearest spheres. In this case, all the Mie coefficients are site independent. Then, the dipole approximation Eq. (3) reads as

$$\frac{a^j_{m1}}{\bar{a}_1} + \sum_{l=1(l\neq j)}^{N}\sum_{\mu=-1}^{1}(A^{lj}_{m1\mu1}a^l_{\mu1} + B^{lj}_{m1\mu1}b^l_{\mu1}) = -B^{j0}_{m101},$$

$$\frac{b^j_{m1}}{\bar{b}_1} + \sum_{l=1(l\neq j)}^{N}\sum_{\mu=-1}^{1}(A^{lj}_{m1\mu1}b^l_{\mu1} + B^{lj}_{m1\mu1}a^l_{\mu1}) = -A^{j0}_{m101}. \tag{9}$$

We define $\bar{a}_1, \bar{b}_1$ as the dipole Mie coefficients. Solving system of Eq. (9), one can find the coefficients a^j_{m1} and b^j_{m1}. Then, using Eq. (7), one can calculate the polarization amplitude (8).

B. Determination of the dispersion law

To give a relevant physical interpretation of the numerical simulation, we will need the dispersion law for polaritons. If the radius of the ring R is large enough, a traveling polariton can be described in terms of plane waves. For this reason, the dispersion law for a polariton in a linear periodical chain is used instead of the true polariton dispersion law inherent in the ring.

According to the Bloch theorem, a polariton, propagating along a linear chain with the permittivity varying periodically along the z axis, is described by a superposition of plane waves with momenta $q_z = k + 2\pi n/a$, where the quasiwave vector $|k| < \pi/a$, a is the period of the chain, n is integer. For the even N_r, $-N_r/2 < n < N_r/2$. If the dispersion law is $\omega(k)$, the radiationless modes exist only for k obeying the guided mode criterion [15–17,29,30]

$$\frac{\omega(k)}{c} < |k| < \frac{\pi}{a}. \tag{10}$$

Otherwise, the modes are unstable with respect to emission of a free photon. Certainly, condition (10) may only be satisfied if $\omega/c < \pi/a$. Below, we set the speed of light as $c = 1$.

According to the Bloch theorem, the partial amplitudes in the infinite chain may be represented in the form

$$a^j_{mn} = a_{mn}e^{ikx_j}, \quad b^j_{mn} = b_{mn}e^{ikx_j}, \tag{11}$$

where $x_j = aj$ is the coordinate of the center of the j-th particle in the chain.

By substituting Eq. (11) into Eqs. (3) and putting the right-hand side of Eq. (3) equal to zero, one obtains

$$\frac{a_{mn}}{\bar{a}_n} + \sum_{\nu=1}^{+\infty}\sum_{\mu=-\nu}^{\nu}[A_{mn\mu\nu}(\omega,k)a_{\mu\nu} + B_{mn\mu\nu}(\omega,k)b_{\mu\nu}] = 0,$$

$$\frac{b_{mn}}{\bar{b}_n} + \sum_{\nu=1}^{+\infty}\sum_{\mu=-\nu}^{\nu}[A_{mn\mu\nu}(\omega,k)b_{\mu\nu} + B_{mn\mu\nu}(\omega,k)a_{\mu\nu}] = 0. \tag{12}$$

Here

$$A_{nm\mu\nu}(\omega,k) = \sum_{l\neq j} A^{lj}_{nm\mu\nu}e^{ik(x_l - x_j)},$$

$$B_{nm\mu\nu}(\omega,k) = \sum_{l\neq j} B^{lj}_{nm\mu\nu}e^{ik(x_l - x_j)}.$$

Equation (12) form a homogeneous system of linear equations with respect to the partial amplitudes $a_{\mu\nu}$, $b_{\mu\nu}$. They define the dispersion law $\omega(k)$ implicitly. The numerical Newton–Raphson method is used to solve Eq. (12) [14–17].

In a particular case of transverse magnetic modes with $m = n = 1$ [16,17], one has for the dipole approximation

$$\frac{a_{11}}{\bar{a}_1} + A_{1111}(\omega,k)a_{11} + B_{1111}(\omega,k)b_{11} = 0,$$

$$\frac{b_{11}}{\bar{b}_1} + A_{1111}(\omega,k)b_{11} + B_{1111}(\omega,k)a_{11} = 0. \tag{13}$$

Here

$$A(B)_{1111}(\omega,k) = \sum_{l\neq j} A(B)^{lj}_{1111}e^{ik(x_l - x_j)}.$$

The nontrivial solution of Eq. (13) exists if

$$\left[\frac{1}{\bar{a}_1} + A_{1111}(\omega,k)\right]\left[\frac{1}{\bar{b}_1} + A_{1111}(\omega,k)\right] - [B_{1111}(\omega,k)]^2 = 0. \tag{14}$$

We will apply Eq. (14) to the ring that contains N_r particles. For this reason, the wave vector k runs the values $k_p = 2\pi p/N_r a$, where the wave number p is integer, $-N_r/2 < p < N_r/2$.

IV. RESULTS

To study the light propagating through the two-port ring waveguide, we consider, as an example, the case $N_r = 80$ and $N_c = 20$ (see Fig. 1). The waveguide is composed of identical spherical GaAs particles with refractive index $n_r = 3.5$. In the system of units used below, we consider particles of diameter $a = 2$.

It follows from our previous publications that, if the number of particles is large enough, both linear and circular arrays composed of the same particles possess practically identical pass bands and high-quality modes [14,16,17]. For this reason, we are interested in the light source frequencies inherent in the pass band. Let us recall that we are interested in

the pass band corresponding to dipole magnetic transverse modes. The upper limit for this band, in our system of units, is $\omega_{up} \approx 0.843$ [17]. We will investigate in detail the frequency region adjacent to the upper edge of the pass band since these modes have the highest quality factor.

Before studying the two-port ring waveguide, let us first investigate more simple ring waveguide. Let us place the light source near the particle B (see Fig. 2). The goal is to calculate the polariton intensity inside an arbitrary particle C.

The calculation scheme is the following. Frequency ω that belongs to the pass band is chosen for the point source. Then, the Mie coefficients and the vector translation coefficients in Eq. (9) are calculated. This defines Eq. (9) in the dipole approximation completely. The solution of these equations gives the partial amplitudes $a^j_{\mu 1}$ and $b^j_{\mu 1}$. Using Eqs. (6) and (7), one can find the polarization vector $\mathbf{P}^j(\mathbf{r})$ [see. Eq. (8)].

Consider the behavior of $\mathbf{P}^j(\mathbf{r})$ for the ring of radius R. It is convenient to characterize a position on the ring by the angle α (see Fig. 2). Then, the polarization intensity is determined as follows:

$$I(\alpha) = |\mathbf{P}^j(\mathbf{r})|^2. \tag{15}$$

The frequencies of the pass band form a quasicontinuous spectrum. We start with the frequency $\omega \approx 0.844$, and decrease it with the step $\Delta\omega = 10^{-8}$. As a result, one finds that the intensity $I(\alpha)$ reveals an interesting feature for certain frequencies. The intensity $I(\alpha)$ experiences modulation with a period of several tens of particles. In the dipole approximation, first several highest frequencies for which the effect takes place are $\omega_1 \approx 0.8431$, $\omega_2 \approx 0.8424$, $\omega_3 \approx 0.8413$, and $\omega_4 \approx 0.8397$. In the quadrupole approximation, these are $\omega'_1 \approx 0.8399$, $\omega'_2 \approx 0.8393$, $\omega'_3 \approx 0.8384$, and $\omega'_4 \approx 0.8370$. Deviation from these resonant frequencies by 0.1% strongly reduces the signal amplitude and also makes the angular dependence $I(\alpha)$ chaotic. To understand better these resonant frequency magnitudes, let us calculate the wave vectors which correspond to resonant frequencies. Using the algorithm described in Sec. III B, one finds that the modes ω_1, ω'_1 possess wave number $p=39$, modes ω_2, ω'_2 possess wave number $p=38$, modes ω_3, ω'_3 possess wave number $p=37$, etc. Thus, the frequencies for which the effect takes place are resonant ones corresponding to normal modes of the ring.

As an example, consider in detail the modes corresponding to the wave number $p=38$. In Fig. 3, the dependence of the intensity $I(\alpha)$ is presented. The thin solid curve and the thin dashed curve correspond to the dipole and quadrupole approximations, respectively.

The intensity manifests strong oscillations on the scale of the order of the interparticle distance or $\delta\alpha = 2\pi/N_r$. As one should expect, the peaks on the thin curves correspond to the angles $\alpha_j = j \cdot \delta\alpha$, $j = 1, \ldots, N_r$. A remarkable feature of these curves is a noticeable amplitude modulation of the intensity. The period of this modulation is approximately 20 particles or $20 \cdot \delta\alpha$. Let us clarify this feature.

It is evident that inside every j-th sphere the intensity $I(\alpha)$ is proportional to the j-th partial amplitudes. In particular, let it be b^j_{01}. The triangles and squares in Fig. 3 correspond to the polarization intensity $I(\alpha_j) \sim I^{\alpha_j}_b \sim |b^j_{01}|^2$ found in the dipole and quadrupole approximations, respectively. Further, let us define the average intensity as follows

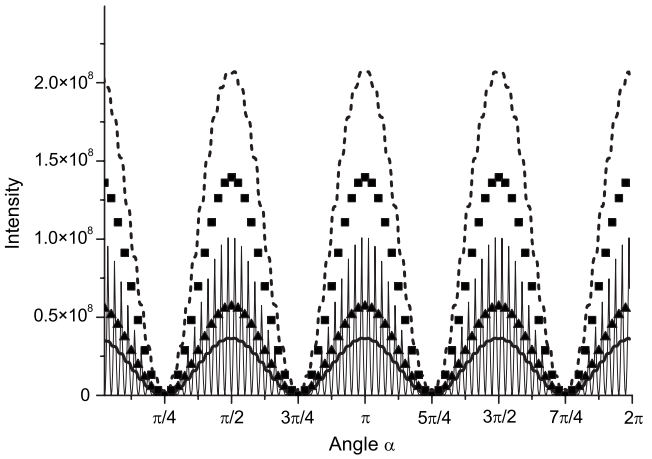

FIG. 3. Intensity $I(\alpha)$ for the mode $p=38$ in a *ring* waveguide. The thin solid curve represents the intensity for the dipole approximation. The thick curves correspond to the averaged intensity $\overline{I(\alpha)}$. The triangles and squares correspond to the intensity $I^{\alpha_j}_b$ calculated for the dipole and quadrupole approximations, respectively.

$$\overline{I(\alpha)} = \frac{\int_{\alpha-\delta\alpha/2}^{\alpha+\delta\alpha/2} d\alpha I(\alpha)}{\delta\alpha}. \tag{16}$$

The plot of $\overline{I(\alpha)}$ is shown in Fig. 3 by the thick solid and thick dashed curves in the dipole and quadrupole approximations, respectively.

One can make some immediate observations based on Fig. 3. First, the curve $\overline{I(\alpha)}$ well approximates the intensities I^j_b. Second, the period of amplitude modulation is practically insensitive to the approximation. For this reason, in the following figures we present only approximate curves for the polarization intensities $I^{\alpha_j}_b$ in the dipole approximation.

Figure 4 shows the approximate curves of the intensity $I^{\alpha_j}_b$

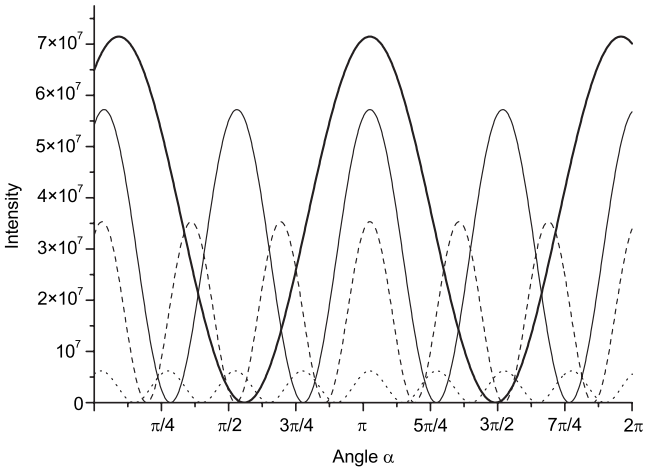

FIG. 4. The intensities $I^{\alpha_j}_b$ for the modes $p_1=39$ (thick solid curve), $p_2=38$ (thin solid curve), $p_3=37$ (dashed curve), and $p_4=36$ (dotted curve) in the circle waveguide.

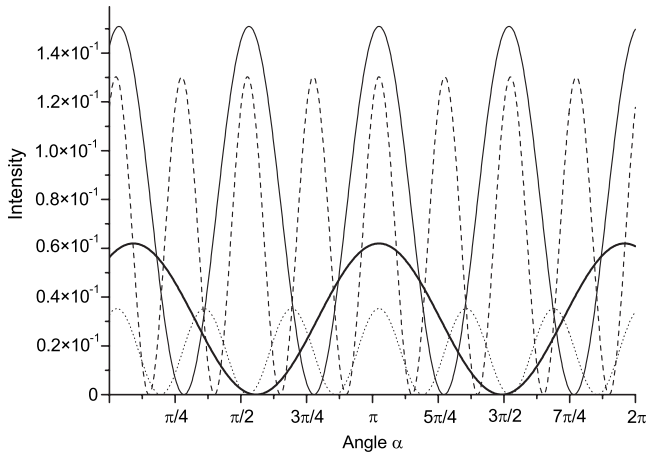

FIG. 5. The intensity $I_b^{\alpha_j}$ at the exit of the two-port waveguide (point D in Fig. 1) for the modes with $p_1=39$ (thick solid curve), $p_2=38$ (thin solid curve), $p_3=37$ (dashed curve), and $p_4=36$ (dotted curve).

for the subsequent frequencies $\omega_1=0,8431$, $\omega_2=0.8424$, $\omega_3=0.8413$, and $\omega_4=0.8397$ corresponding to the wave numbers $p_1=39$, $p_2=38$, $p_3=37$, $p_4=36$, respectively.

Let us turn now to the two-port ring waveguide. In Fig. 5, we presented the approximating curves for the intensity $I_b^{\alpha_j}$ at the end of the output chain CD as function of the angle α between the chains AB and CD.

All Figs. 3–5 reveal the same feature, the distance between the peaks is several tens of the interparticle distance for the resonant frequencies belonging to the pass band. However, the intensity of the peaks for the ring and two-port ring waveguide differ significantly. Below we will give the interpretation of the results obtained.

V. DISCUSSION

In the previous section we have seen that for resonant frequencies, the ring and two-port ring waveguides manifest a remarkable feature. The intensity Eq. (16) of a traveling polariton is quasiperiodic, with the quasiperiod being of the order of several tens of the interparticle distance a.

The polariton frequency induced by the external source coincides with the frequency of the source. Suppose this frequency is ω. The polariton wave vector k corresponding to this frequency is a solution of Eq. (14).

Consider the behavior of intensity in the circular array (Fig. 2). Let $x=0$ for the point B. Using the scalar approximation, a monochromatic wave with the frequency ω traveling clockwise along the ring may be described as a Bloch wave $u_k(x)\exp\{ikx\}$, while a wave traveling counterclockwise is described by function $u_k(L-x)\exp\{ik(L-x)\}$, where x is the length of the arc proportional to angle α and $L=N_r a$ is the total length of the ring. According to the Bloch theorem, $u_k(x)$ is a periodic function: $u_k(x)=u_k(x+a)$. If the two waves traveling in the opposite directions interfere at point x, the polariton amplitude becomes

$$A(x) \propto u_k(x)\exp\{ikx\} + u_k(L-x)\exp\{ik(L-x)\}. \quad (17)$$

This function describes the intensity of the field at any point. Let us consider the intensity at the integer points of the ring $x_j \approx a(j-1)$. Taking into account that $u_k(x_j)=u_k(L-x_j) \equiv \text{const}$, one obtains

$$A(x_j) \propto \exp\{ikx_j\} + \exp\{ik(L-x_j)\}, \quad (18)$$

and the intensity becomes

$$I(\alpha_j) = I_k(x_j) = |A(x_j)|^2 \propto |\exp\{ikx_j\} + \exp\{ik(L-x_j)\}|^2 \propto \cos^2(kx_j), \quad (19)$$

$k=2\pi p/aN_r$. For the integer point x_j, one can replace p by $N_r/2-p$ on the RHS of Eq. (19). Thus,

$$I(\alpha_j) \propto \cos^2\left[\frac{2\pi}{aN_r}\left(\frac{N_r}{2}-p\right)x_j\right], \quad (20)$$

or

$$I(\alpha_j) \propto \cos^2\left[\frac{2\pi(j-1)}{N_r}\left(\frac{N_r}{2}-p\right)\right]. \quad (21)$$

Let us replace p in Eq. (21) subsequently by the values $p_1=39$, $p_2=38$, $p_3=37$, and $p_4=36$. One can see that the dependence Eq. (21) is consistent with the all curves in Figs. 3 and 4. Thus, the results obtained for the ring can be treated in terms of a superposition of two Bloch polaritons moving in the opposite directions along the ring.

Now we can turn to the interpretation of the results obtained for the two-port ring waveguide. The light source excites a polariton at the point A. The polariton travels along AB and then it splits into two waves moving from B to C in different directions. At C these waves interfere with each other and the rejoined polariton travels to D. As the region around the point B (and C as well) is a complex aggregate, our interpretation is not valid for several spheres adjacent to these regions. However, it works quite well for particles separated from these regions by several interparticle distances.

It is remarkable that the polariton intensities differ by many orders of magnitude for the ring and the two-port ring. The large polariton intensity in the case of the ring is because the interference takes place not only for two waves meeting at the point C. The wave traveling clockwise (as well as the wave traveling counterclockwise) revolves along the ring many times. Each time the wave reaches the point C, it contributes to the interference, resulting in the multiple interference.

In the case of the two-port ring, the regions near B and C contribute an extra phase shift and, thus, the multiple interference is destroyed. This explains the huge quantitative difference between the polariton amplitudes for the ring and for the two-port ring. One should pay attention that the mode with $p_1=39$ has the intensity at the output of the two-port ring two orders of magnitude smaller as compared to the other modes. We have no reasonable explanation to this fact. However, the dependence reveals the expected periodicity. We have verified that the weak absorption induced by possible $\text{Im}\, n_r < 0.01$ does not affect qualitatively the interference behavior.

VI. CONCLUSION

In this work, we have investigated the interference of guided polaritons in the ring and two-port ring waveguide composed of dielectric spherical particles. The interference occurs if the frequency of the external source coincides with one of the resonant modes of the ring. We have demonstrated that the angular dependence for the polariton intensity for the ring (Figs. 3 and 4) as well as the transmitted intensity for the two-port ring (Fig. 5) may be well described as interference of scalar waves.

The interference predicted in the paper can be used to control the output (transmitted) intensity by varying the system geometry and the mode frequency. This allows to narrow the transmitted signal in the frequency domain. The interference effect described above may also have a number of other interesting applications including, for instance, filtering and selective enhancement of a guided signal. These results can also be applied to investigating subwavelength waveguides made of metal particles [12,13] in spite of characteristic absorption by conducting electrons.

It is difficult to apply our results directly to experiments on the whispering gallery modes in the arrays of polystyrene particles [1] because the dipole approach is irrelevant for the modes with large angular momenta. However, interference effects may be seen there because the coupling of spheres is essentially a local phenomenon [2]. Another interesting application can be considered regarding the propagation of microwaves in the arrays of coupled antennas [5,18], which are very similar to our particle aggregates. Interference can be used there for the frequency selective emission, absorption or transport of the microwave signal.

ACKNOWLEDGMENTS

This work is supported by the Air Force Office of Scientific Research (Award No. FA 9550-06-1-0110), Russian Federal Science and Innovation Program (Award No. 2008-10-1.3-07-21-031), and the Russian Fund for Basic Research. The authors acknowledge fruitful discussions with Yu. Kagan, Vasilii Asratov, Mark Sulkes, and Arthur Yahjian.

[1] V. N. Astratov, J. P. Franchak, and S. P. Ashili, Appl. Phys. Lett. **85**, 5508 (2004).
[2] L. I. Deych and O. Roslyak, Phys. Rev. E **73**, 036606 (2006).
[3] B. M. Möller, U. Woggon, and M. V. Artemyev, Opt. Lett. **30**, 2116 (2005).
[4] Y. Hara, T. Mukaiyama, K. Takeda, and M. Kuwata-Gonokami, Phys. Rev. Lett. **94**, 203905 (2005).
[5] R. A. Shore and A. D. Yaghjian, Electron. Lett. **41**, 578 (2005).
[6] S. Fan, J. N. Winn, A. Devenyi, J. C. Chen, R. D. Meade, and J. D. Joannopoulos, J. Opt. Soc. Am. B **12**, 1267 (1995).
[7] R. D. Meade, A. M. Rappe, K. D. Brommer, J. D. Joannopoulos, and O. L. Alherhand, Phys. Rev. B **48**, 8434 (1993).
[8] Z. Y. Tang and N. A. Kotov, Adv. Mater. **17**, 951 (2005).
[9] S. A. Maier, P. G. Kik, and H. A. Atwater, Phys. Rev. B **67**, 205402 (2003).
[10] L. A. Sweatlock, S. A. Maier, H. A. Atwater, J. J. Penninkhof, and A. Polman, Phys. Rev. B **71**, 235408 (2005).
[11] M. L. Brongersma, J. W. Hartman, and H. A. Atwater, Phys. Rev. B **62**, R16356 (2000).
[12] S. A. Maier, P. G. Kik, H. A. Atwater, S. Meltzer, E. Harel, B. E. Koel, and A. A. G. Requicha, Nature Mater. **2**, 229 (2003).
[13] S. A. Maier, M. L. Brongersma, P. G. Kik, S. Meltzer, A. A. G. Requicha, B. E. Koel, and H. A. Atwater, Adv. Mater. **15**, 562 (2003).
[14] A. L. Burin, Phys. Rev. E **73**, 066614 (2006).
[15] A. L. Burin, G. C. Schatz, H. Cao, and M. A. Ratner, J. Opt. Soc. Am. B **21**, 121 (2004).
[16] Gail S. Blaustein, Michael I. Gozman, Olga Samoylova, I. Ya. Polishchuk, and Alexander L. Burin, Opt. Express **15**, 17380 (2007).
[17] Michael I. Gozman, I. Ya. Polishchuk, and Alexander L. Burin, Phys. Lett. A **372**, 5250 (2008).
[18] R. W. P. King, G. J. Fikioris, and R. B. Mack, *Cylindrical Antennas and Arrays* (Cambridge University Press, Cambridge, England, 2005).
[19] D. K. Freeman and T. T. Wu, IEEE Trans. Antennas Propag. **43**, 340 (1995).
[20] E. I. Smotrova and A. I. Nosich, Opt. Quantum Electron. **36**, 213 (2004); S. V. Boriskina, T. M. Benson, P. Sewell, and A. I. Nosich, IEEE J. Quantum Electron. **41**, 857 (2005).
[21] G. K. Gopalakrishnan and K. Chang, Electron. Lett. **30**, 148 (1994).
[22] K. Chang, S. Martin, F. Wang, and J. L. Klein, IEEE Trans. Microwave Theory Tech. **35**, 1288 (1987).
[23] J. R. Bray and L. Roy, IEEE Trans. Microwave Theory Tech. **51**, 1540 (2003).
[24] E. D. Palik, *Handbook of Optical Constants in Solids* (Academic, New York, 1985).
[25] Y. L. Xu, Appl. Opt. **36**, 9496 (1997).
[26] Y. L. Xu, J. Opt. Soc. Am. A Opt. Image Sci. Vis **20**, 2093 (2003).
[27] Y. L. Xu and R. T. Wang, Phys. Rev. E **58**, 3931 (1998).
[28] The relations below differ from those in [25,26] where the scattering of the plane wave was considered.
[29] Yu. Kagan and V. M. Afanas'ev, Zh. Eksp. Teor. Phys. **50**, 271 (1966) [Sov. Phys. JETP **23**, 178 (1966)].
[30] V. M. Agranovich and O. A. Dubovskii, Pis'ma Zh. Eksp. Teor. Fiz. **3**, 345 (1966) [JETP Lett. **3**, 223 (1966)].